Conducting Materials

DOI: 10.1002/anie.201106203

High-Rate Charge-Carrier Transport in Porphyrin Covalent Organic Frameworks: Switching from Hole to Electron to Ambipolar Conduction**

Xiao Feng, Lili Liu, Yoshihito Honsho, Akinori Saeki, Shu Seki, Stephan Irle, Yuping Dong, Atsushi Nagai, and Donglin Jiang**

Conducting polymers play a key role in optoelectronics, transistors, and solar cells owing to their capability in charge-carrier transport. To achieve high-rate carrier transport, the molecular design of a conjugated structure that allows the formation of organized conducting pathways is highly preferred.[1] In this context, two-dimensional covalent organic frameworks (2D COFs) offer a new class of conducting polymers with unconventional structures that feature 2D polygon sheets and eclipsed stacking architecture to provide preorganized pathways for charge-carrier transport.[2,3] A significant feature of COFs is that the ordering of building blocks in the 2D polygon sheet is discrete and the layered alignment of 2D sheets is parallel and unidirectional. Such a well-organized architecture with precise intra- and interplane orderings is seldom available with conventional 1D and 3D conducting polymers.

We have focused on the synthesis of π-electronic 2D COFs by integrating π-electronic components into the skeletons of 2D COFs.[3] Recently, we have developed a typical and large π system, that is, a porphyrin unit for the synthesis of a tetragonal 2D porphyrin COF, which shows high crystallinity and large surface area.[4] During the course of the study, we found that the porphyrin units stacked in an eclipsed mode and formed conduction pathways that enable high-rate charge-carrier conduction. Interestingly, the types of charge carriers that can move in the 2D COFs are dominated by the central metals in the porphyrin rings, thus allowing the switching of conducting nature from hole to electron as well as to ambipolar, based on the same 2D COF architecture (Figure 1, MP-COF, M = H_2, Zn, and Cu). Herein we report the synthesis, structure, and high-rate carrier transporting properties of porphyrin COFs and highlight their functions in switching their conducting nature and their drastic effects on the photoconductivity of COFs.

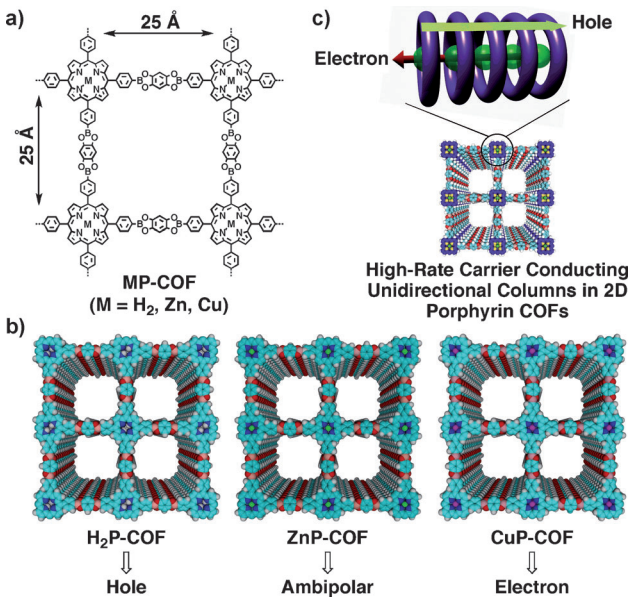

Figure 1. a) Schematic representation of MP-COFs (M = H_2, Zn, and Cu). b) Schematic graphs of a 2×2 grid of MP-COFs with achiral AA stacking 2D sheets (C: light blue; N: deep blue; H: white; O: red; B: pink; Zn: green; Cu: violet). c) Graphical representation of metal-on-metal and macrocycle-on-macrocycle channels for respective electron and hole transport in stacked porphyrin column of 2D porphyrin COFs.

2D porphyrin COFs, that is, H_2P-COF, ZnP-COF, and CuP-COF, with free base, zinc, and copper porphyrin units at the nodes of a tetragonal mesoporous framework were newly synthesized and unambiguously characterized by spectroscopy (see Figures S1–S3 in the Supporting Information). Field-emission scanning electron microscopy (FE/SEM) showed that H_2P-COF, ZnP-COF, and CuP-COF adopted disk, cube,

[*] X. Feng, Dr. A. Nagai, Prof. Dr. D. Jiang[+]
Department of Materials Molecular Science, Institute for Molecular Science, National Institutes of Natural Sciences
5-1 Higashiyama, Myodaiji, Okazaki 444-8787 (Japan)
E-mail: jiang@ims.ac.jp
L. Liu, Prof. Dr. S. Irle, Prof. Dr. D. Jiang[+]
Department of Chemistry, Graduate School of Science
Nagoya University, Furo-cho, Chikusa-ku, Nagoya 464-8601 (Japan)
E-mail: sirle@iar.nagoya-u.ac.jp
Y. Honsho, A. Saeki, Prof. Dr. S. Seki
Department of Applied Chemistry, Graduate School of Engineering
Osaka University, Osaka 565-0871 (Japan)
X. Feng, Prof. Y. Dong
College of Materials Science and Engineering
Beijing Institute of Technology, Beijing 100081 (P.R. China)
[+] Precursory Research for Embryonic Science and Technology (PRESTO)
Japan Science and Technology Agency (JST)
Chiyoda-ku, Tokyo 102-0075 (Japan)

[**] This work is supported by Precursory Research for Embryonic Science and Technology (PRESTO) (Japan) from the Science and Technology Agency (JST) (D.J.).
Supporting information for this article is available on the WWW under http://dx.doi.org/10.1002/anie.201106203.

and belt morphologies, respectively (see Figure S4 in the Supporting Information). High-resolution transmission electron microscopy (HR/TEM) of ZnP-COF revealed that each line is straight and represents a single 2D sheet that stacks at the same interval to form a layered structure (see Figure S4). Direct visualization of the tetragonal texture with HR/TEM was successful and the pore size was estimated to be 2.5 nm, which was close to the theoretical value.

We obtained a fully optimized molecular structure, stacking energies, atomic charges, and orbital energies of 2D porphyrin COF stacks using the carefully benchmarked dispersion-corrected density-functional tight-binding (DFTB) method. The AA stacking alignment has a total crystalline stacking energy of 263.6 kcal mol^{-1} per monolayer unit, which is larger than the AB stacking alignment (see Table S1 in the Supporting Information). The c lattice constant in the case of AB stacking is 3.3 Å, which is dramatically shorter than that in the case of the AA stacking alignment with an interlayer spacing of 3.9 Å. Despite a smaller c value, the AB stacking energy (Lennard-Jones crystal stacking energy) is only 144.7 kcal mol^{-1}, which is about 55 kcal mol^{-1} smaller than that of the AA stacking alignment (199.9 kcal mol^{-1}). Upon AA stacking, the dihedral angle between bridge and porphyrin plane decreases from 90° in the monolayer to approximately 45° in the stacked layers, thus indicating that the π-stacking interaction forces the system to overcome the steric repulsion between the *ortho*-hydrogen atoms. The porphyrin node shows chiral, achiral, and C_2 isomers having different orientations of the four phenyl groups (Figure 2a). These isomers cannot interconvert because of the existence of large rotational barriers of the bridges that are in excess of 150 kcal mol^{-1}; such rotation is severely hindered in the AA stack. We found that only stacks with identical bridge rotation isomers aggregate on top of each other, and mixed combinations cannot be realized as a result of severe stacking defects. Interestingly, the achiral AA stacking was found to be the most stable structure (Figures 2b–d, and see Table S1), with a stacking energy that is approximately 86 and 36 kcal mol^{-1} per monolayer unit more stable than that for the chiral AA and C_2 AA stacking structures, respectively (for atomistic coordinates see CIF files in the Supporting Information). As shown in Figures 2b–d, a decrement in net charge of the porphyrin macrocycle was observed for ZnP-COF and CuP-COF, in comparison with H_2P-COF, as a result of metal coordination.

The intense X-ray diffraction (XRD) peaks for MP-COFs at $2\theta = 3.5°$ were consistent with the above-mentioned stacking structure and assignable to regularly ordered mesopores in a tetragonal orientation with a d_{200} spacing value of 25 Å (Figures 3a–c, green curves). The XRD peaks corresponding to d_{001} spacing appeared at $2\theta = 23°$, which gave the distance between layers to be 3.9 Å. Pawley refinements of the observed XRD profiles using the Reflex Plus module of the Materials Studio version 4.4 suite of programs gave XRD patterns (Figure 3a–c, red curves) and confirmed the assignment of observed reflections. All of the refined profiles were consistent with the experimentally observed XRD patterns, as evidenced by very small differences (Figure 3a–c, black curves). The simulated XRD pattern based on optimized achiral AA unit-cell structures (see Table S2 in the Supporting Information) matched the experimental peak positions and intensities reasonably well (Figure 3a–c, blue curves). In agreement with the structure simulation results, the 2D sheets stack to form periodically ordered porphyrin columns interwoven at 2.5 nm separation along the x and y directions, while

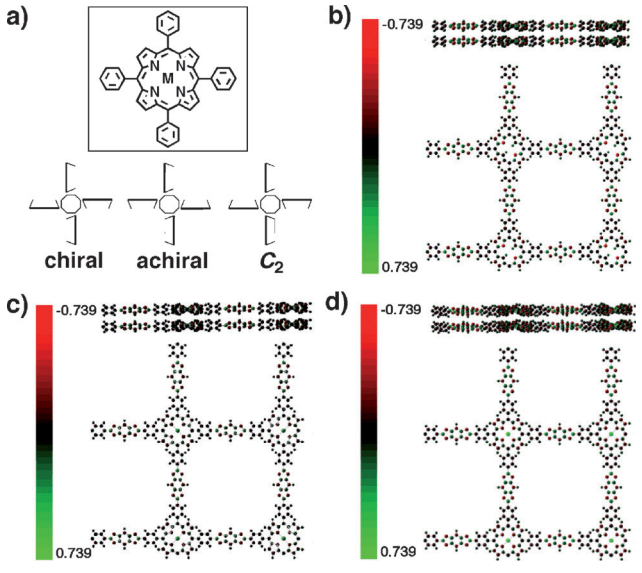

Figure 2. a) Schematic representation of chiral, achiral, and C_2 isomers of porphyrins having different orientations of the four phenyl groups. Achiral AA stacking structures of H_2P-COF (b), ZnP-COF (c), and CuP-COF (d). The color of the atoms in b–d are consistent with their net charges (color bars).

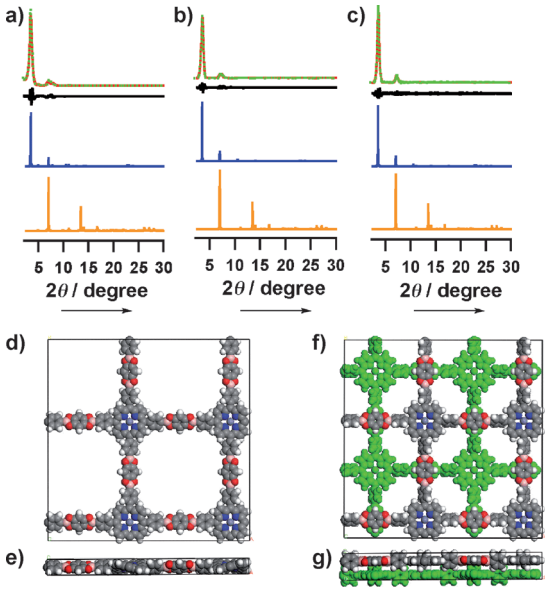

Figure 3. XRD patterns of H_2P-COF (a), ZnP-COF (b), and CuP-COF (c). The experimentally observed: green; the Pawley refinement: red; their difference: black; the simulation of achiral AA stacking model: blue; the simulation of AB stacking model: orange. Views of the unit cell derived from achiral AA stacking model along the z (d) and y (e) axes of ZnP-COF. Views of the unit cell derived from AB stacking model along the z (f) and y (g) axes of ZnP-COF.

in the z direction, each column consists of unidirectional porphyrin-on-porphyrin and metal-on-metal stacks with an interlayer distance of 3.9 Å (Figures 3 d,e). In contrast, the staggered achiral AB stacking alignment did not match the experimentally observed patterns (Figures 3 a–c, orange curves). In this case, the porphyrin sheet overlaps on the pore of the neighboring sheet (Figures 3 f,g).

Nitrogen sorption isotherm measurements at 77 K were carried out for the evaluation of porous structure. All of the porphyrin COFs exhibited almost identical type IV reversible sorption isotherm curves, which is characteristic of mesoporous materials (Figures 4 a–c, blue curves). Analysis of the sorption curves of H_2P-COF, ZnP-COF, and CuP-COF by the

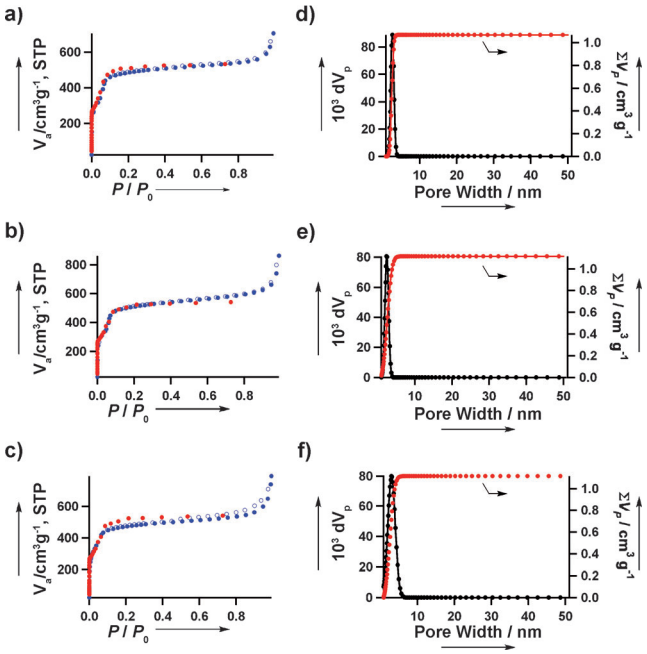

Figure 4. Nitrogen sorption isotherm curves for H_2P-COF (a), ZnP-COF (b), and CuP-COF (c) at 77 K. Experimentally measured curve: blue; GCMC simulated curve based on the achiral AA stacking model: red. Pore size (black, left axis) and pore-size distribution profiles (red, right axis) for H_2P-COF (d), ZnP-COF (e), and CuP-COF (f), respectively.

Brunauer-Emmett-Teller (BET) method gave specific surface areas of 1894, 1713, and 1724 $m^2 g^{-1}$, respectively. Evaluations of pore size with a nonlocal density-functional theory (NLDFT) model indicated a common pore width of 2.5 nm (Figures 4 d–f, black curves), which was the same as the theoretical value (2.5 nm). The pore distribution profiles confirmed that the surface area originates from persistent mesopores (Figure 4 d–f, red curves). To assess the perfectness of the pores, grand canonical Monte Carlo (GCMC) methods were employed for simulation of the nitrogen sorption isotherm curves based on the crystalline models of the achiral AA stacks.[5] The experimentally observed adsorption curves are in good agreement with the simulated curves (Figure 4 a–c, red curves). The surface areas of H_2P-COF, ZnP-COF, and CuP-COF determined from the GCMC simulations were 1901, 1781, and 1779 $m^2 g^{-1}$, respectively, which indicate that the mesoporous porphyrin COFs are close to their theoretical porosities.

Flash-photolysis time-resolved microwave conductivity (FP/TRMC) methods, which allow measurement of the intrinsic charge-carrier mobility to within several nanometers after laser pulse irradiation under a rapidly oscillating electric field, was utilized to quantitatively evaluate the charge-carrier transport in the COFs.[6] The electrodeless FP/TRMC method can minimize the influence of factors such as impurities, chemical and physical defects, and organic/electrode interfaces, as compared to the time-of-flight (TOF) and field-effect transistor (FET) methods. Moreover, FP/TRMC measurements under an argon atmosphere enables elucidation of the total carrier mobilities ($\Sigma\mu_{total}$), including both electrons and holes, whereas using a SF_6 atmosphere gives only hole mobilities (μ_h) as electrons are trapped by SF_6. Therefore, both the intrinsic carrier mobilities of holes and electrons can be obtained using the FP/TRMC technique.

Upon laser flash, rise and decay profiles of the FP/TRMC signal, given by $\phi\Sigma\mu$, are observed, where ϕ and $\Sigma\mu$ represent the photocarrier generation yield and the sum of the generated charge carrier mobities, respectively (see Figures S5a-c in the Supporting Information). The maximum value of $\phi\Sigma\mu$ is generally used for evaluation of the photoconductivity of a material. H_2P-COF displays hole transport ($\phi\mu_h = 1.8\times10^{-4}\,cm^2V^{-1}s^{-1}$), to give the same values of transient conductivities measured under Ar and SF_6 atmospheres (Figure S5a). In sharp contrast, CuP-COF favors electron transport, as indicated by the $\phi\mu_e$ value of $1.16\times10^{-4}\,cm^2V^{-1}s^{-1}$, which is much larger than the $\phi\mu_h$ value of $3.68\times10^{-5}\,cm^2V^{-1}s^{-1}$ (Figure S5b). In contrast, ZnP-COF exhibits comparable carrier mobilities for both holes and electrons ($\phi\mu_e = 5.4\times10^{-5}\,cm^2V^{-1}s^{-1}$, $\phi\mu_h = 3.36\times10^{-5}\,cm^2V^{-1}s^{-1}$; Figure S5c).

Time-of-flight transient current integration measurements revealed that the maximum quantum yield (ϕ) of photocarrier generation for H_2P-COF was 5×10^{-5} (see Figure S5d in the Supporting Information). Therefore, the minimum μ_h value was calculated to be as high as 3.5 $cm^2V^{-1}s^{-1}$, which is twofold as high as that of phthalocyanine COF (1.6 $cm^2V^{-1}s^{-1}$). This μ_h value is much higher than those of small organic semiconductors, conjugate polymers, and self-assembly systems as measured by the FP/TRMC method.[7] Theoretical calculations on triphenylene-based COF-5 indicate that the hole transport through stacking triphenelene columns is a bandlike motion process, which allows much faster transport than those of liquid-crystalline-orientated molecular systems.[8] The ϕ value of ZnP-COF was estimated to be 1.9×10^{-3} by the transient absorption spectroscopic method, and the μ_e and μ_h values were 0.016 and 0.032 $cm^2V^{-1}s^{-1}$, respectively. In contrast, the ϕ value of CuP-COF was 6×10^{-4}, which led to the minimum electron mobility of 0.19 $cm^2V^{-1}s^{-1}$. Therefore, 2D porphyrin COFs are high-rate conducting COFs wherein the metal ions in porphyrins determine the type of charge carrier that can move in the columns and regulate the ease of carrier motion within the frameworks. We highlight that H_2P-COF is a top class high-rate hole-transporting COF and ZnP-COF is the first example of ambipolar conducting COFs.

The AA stacking offers macrocycle-on-macrocycle and metal-on-metal pathways within porphyrin columns. Similar structures have been observed for single crystals of metallomacrocycles.[9] The metal-on-metal ordering in the crystals leads to the formation of two channels for carrier motion, that is, macrocycle and metal channels (Figure 1c). The hole-conduction nature of H_2P-COF indicates that the stacking macrocycles without central metals form a path for hole transport. Insertion of a metal species to the porphyrin macrocycles gives rise to the formation of the metal-on-metal channel, which accounts for the electron transport. The insertion of a central metal to the porphyrin macrocycle, lowers the electron density of the macrocycles.[10] Calculated partial atomic charges in the unit cell of porphyrin COFs revealed that the electron densities of the porphyrin macrocycles were decreased for ZnP-COF and CuP-COF, as compared to that of H_2P-COF (Figures 3b–d). The decrease in the electron density of porphyrin macrocycles decreases the mobility of holes through the stacked macrocycles. Moreover, copper metal has a strong tendency to exhibit ligand-to-metal charge transfer, thus significantly reducing the electron density of the porphyrin macrocycles.[11] Consequently, CuP-COF favors electron transport through the metal-on-metal channel, whereas the zinc metal is free of ligand-to-metal charge transfer and allows balanced transport through both channels; that is, it becomes an ambipolar conduction.

The distinct conducting nature of MP-COFs has a remarkable effect on their photoconductivity. Upon irradiation with visible light (> 400 nm) using a Xe lamp, all of the porphyrin COFs exhibited photocurrent generation, but their responses are significantly different from one another. For example, ZnP-COF generated a photocurrent of approximately 26.8 nA, whereas CuP-COF and H_2P-COF displayed photocurrents of only 0.6 and 0.01 nA, respectively (Figure 5a and Figure S6 in the Supporting Information). ZnP-COF had the largest on-off ratio of 5×10^4, whereas the ratio was only 300 and 4 for CuP-COF and H_2P-COF, respectively. Therefore, a balanced hole and electron transport drives the high on-off ratio photocurrent production, while the unbalanced carrier transport leads to a low photoconductivity. Along these lines, we additionally investigated the wavelength-dependent response of ZnP-COF, because of its broad absorbance over the solar spectrum. Interestingly, ZnP-COF exhibited prominent photocurrent generation, especially when exposed to long-wavelength visible and near IR lights, such as at $\lambda = 600$, 620, and 700 nm (Figure 5b).

In summary, we have explored porphyrin macrocycles bearing different central metals for the synthesis of high-rate charge carrier conducting 2D COFs. The AA stacking alignment is the most favorable layer structure and offers columnar porphyrin paths, that is, macrocycle-on-macrocycle and metal-on-metal channels, through which holes and electrons are transported within the COFs. Bridge rotational isomers are found to be separated by large barriers that stabilize such isomers up to high temperatures, and we predict that AA stacks possess identical bridge conformations in each layer. The focal metals in the porphyrin rings play a dominating role not only in the formation of channels for electron conduction, but also in the regulation of the ease of carrier motion, thereby leading to the formation of high-rate hole, electron, and ambipolar conducting COFs. The insights into the conducting nature and its remarkable effect on photoconductivity provide guidance for the application of the 2D COFs. For example, pairing MP-COFs with electronically active counterparts trapped in the mesoporous channels would allow the construction of organized donor–acceptor systems. Together with the enhanced absorbance in the visible and IR regions, large carrier mobilities, and high thermal stability, porphyrin-COF-based donor–acceptor systems are a subject worthy of further investigation.

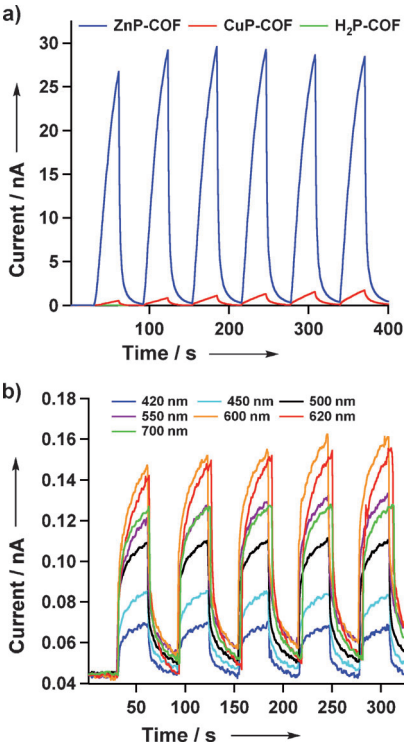

Figure 5. a) Photocurrents for 2D porphyrin COFs upon repeated switching of the light on and off. b) Wavelength-dependent on-off switching of photocurrent of ZnP-COF at a bias voltage of 1.0 V.

Received: September 1, 2011
Revised: November 27, 2011
Published online: January 31, 2012

Keywords: ambipolar materials · conducting materials · covalent organic frameworks · electron transport · porphyrinoids

[1] a) R. Bhosale, J. Misek, N. Sakai, S. Matile, *Chem. Soc. Rev.* **2010**, *39*, 138–149; b) H. Sirringhaus, P. J. Brown, R. H. Friend, M. M. Nielsen, K. Bechgaard, B. M. W. Langeveld-Voss, A. J. H. Spiering, R. A. J. Janssen, E. W. Meijer, P. Herwig, D. M. de Leeuw, *Nature* **1999**, *401*, 685–688; c) Y. Y. Liang, Z. Xu, J. B. Xia, S. T. Tsai, Y. Wu, G. Li, C. Ray, L. P. Yu, *Adv. Mater.* **2010**, *22*, E135–E138; d) S. D. Oosterhout, M. M. Wienk, S. S. van Bavel, R. Thiedmann, L. J. A. Koster, J. Gilot, J. Loos, V. Schmidt, R. A. J. Janssen, *Nat. Mater.* **2009**, *8*, 818–824.

[2] a) A. P. Cote, A. I. Benin, N. W. Ockwig, M. O'Keeffe, A. J. Matzger, O. M. Yaghi, *Science* **2005**, *310*, 1166 – 1170; b) R. W. Tilford, W. R. Gemmill, H. C. zur Loye, J. J. Lavigne, *Chem. Mater.* **2006**, *18*, 5296 – 5301; c) A. P. Côté, H. M. El-Kaderi, H. Furukawa, J. R. Hunt, O. M. Yaghi, *J. Am. Chem. Soc.* **2007**, *129*, 12914 – 12915; d) E. L. Spitler, W. R. Dichtel, *Nat. Chem.* **2010**, *2*, 672 – 677; e) J. W. Colson, A. R. Woll, A. Mukherjee, M. P. Levendorf, E. L. Spitler, V. B. Shields, M. G. Spencer, J. Park, W. R. Dichtel, *Science* **2011**, *228*, 228 – 231; f) M. Dogru, A. Sonnauer, A. Gavryushin, P. Knochel, T. Bein, *Chem. Commun.* **2011**, *47*, 1707 – 1709; g) R. W. Tilford, S. J. Mugavero, P. J. Pellechia, J. J. Lavigne, *Adv. Mater.* **2008**, *20*, 2741 – 2746; h) L. M. Lanni, R. W. Tilford, M. Bharathy, J. J. Lavigne, *J. Am. Chem. Soc.* **2011**, *133*, 13975 – 13983; i) N. L. Campbell, R. Clowes, L. K. Ritchie, A. I. Cooper, *Chem. Mater.* **2009**, *21*, 204 – 206; j) S. Wan, F. Gndara, A. Asano, H. Furukawa, A. Saeki, S. K. Dey, L. Liao, M. W. Ambrogio, Y. Y. Botros, X. Duan, S. Seki, J. F. Stoddart, O. M. Yaghi, *Chem. Mater.* **2011**, *23*, 4094 – 4097; k) E. L. Spitler, B. T. Koo, J. L. Novotney, J. W. Colson, F. J. Uribe-Romo, G. D. Gutierrez, P. Clancy, W. R. Dichtel, *J. Am. Chem. Soc.* **2011**, *133*, 19416 – 19421.

[3] a) S. Wan, J. Guo, J. Kim, H. Ihee, D. Jiang, *Angew. Chem.* **2008**, *120*, 8958 – 8962; *Angew. Chem. Int. Ed.* **2008**, *47*, 8826 – 8830; b) S. Wan, J. Guo, J. Kim, H. Ihee, D. Jiang, *Angew. Chem.* **2009**, *121*, 5547 – 5550; *Angew. Chem. Int. Ed.* **2009**, *48*, 5439 – 5442; c) X. S. Ding, J. Guo, X. A. Feng, Y. Honsho, J. D. Guo, S. Seki, P. Maitarad, A. Saeki, S. Nagase, D. Jiang, *Angew. Chem.* **2011**, *123*, 1325 – 1329; *Angew. Chem. Int. Ed.* **2011**, *50*, 1289 – 1293; d) N. Atsushi, Z. Guo, X. Feng, S. Jin, X. Chen, X. Ding, D. Jiang, *Nat. Commun.* **2011**, *2*, 536; e) X. Ding, L. Chen, Y. Honsho, X. Feng, O. Saengsawang, J. Guo, A. Saeki, S. Seki, S. Irle, S. Nagase, P. Vudhichai, D. Jiang, *J. Am. Chem. Soc.* **2011**, *133*, 14510 – 14513.

[4] X. Feng, L. Chen, Y. P. Dong, D. Jiang, *Chem. Commun.* **2011**, *47*, 1979 – 1981.

[5] N. Metropolis, A. W. Rosenbluth, M. N. Rosenbluth, A. H. Teller, *J. Chem. Phys.* **1953**, *21*, 1087 – 1092.

[6] A. Saeki, S. I. Ohsaki, S. Seki, S. Tagawa, *J. Phys. Chem. C* **2008**, *112*, 16643 – 16650.

[7] a) T. Arnaya, S. Seki, T. Moriuchi, K. Nakamoto, T. Nakata, H. Sakane, A. Saeki, S. Tagawa, T. Hirao, *J. Am. Chem. Soc.* **2009**, *131*, 408 – 409; b) A. Saeki, S. I. Ohsaki, Y. Koizumi, S. Seki, S. Tagawa, *J. Photopolym. Sci. Technol.* **2008**, *21*, 559 – 562; c) S. Prasanthkumar, A. Saeki, S. Seki, A. Ajayaghosh, *J. Am. Chem. Soc.* **2010**, *132*, 8866 – 8867; d) H. Nobukuni, F. Tani, Y. Shimazaki, Y. Naruta, K. Ohkubo, T. Nakanishi, T. Kojima, S. Fukuzumi, S. Seki, *J. Phys. Chem. C* **2009**, *113*, 19694 – 19699.

[8] S. Patwardhan, A. A. Kocherzhenko, F. C. Grozema, L. D. A. Siebbeles, *J. Phys. Chem. C* **2011**, *115*, 11768 – 11772.

[9] a) K. Yakushi, H. Yamakado, T. Ida, A. Ugawa, *Solid State Commun.* **1991**, *78*, 919 – 923; b) T. Inabe, H. Tajima, *Chem. Rev.* **2004**, *104*, 5503 – 5533; c) A. Calzolari, A. Ferretti, M. B. Nardelli, *Nanotechnology* **2007**, *18*, 424013; d) C. J. Schramm, R. P. Scaringe, D. R. Stojakovic, B. M. Hoffman, J. A. Ibers, T. J. Marks, *J. Am. Chem. Soc.* **1980**, *102*, 6702 – 6713; e) J. Martinsen, S. M. Palmer, J. Tanaka, R. C. Greene, B. M. Hoffman, *Phys. Rev. B* **1984**, *30*, 6269 – 6276; f) T. Inabe, S. Nakamura, W. B. Liang, T. J. Marks, R. L. Burton, C. R. Kannewurf, K. Imaeda, *J. Am. Chem. Soc.* **1985**, *107*, 7224 – 7226; g) M. Y. Ogawa, J. Martinsen, S. M. Palmer, J. L. Stanton, J. Tanaka, R. L. Greene, B. M. Hoffman, J. A. Ibers, *J. Am. Chem. Soc.* **1987**, *109*, 1115 – 1121.

[10] a) J. C. De Paula, V. A. Walters, C. Nutaitis, J. Lind, K. Hall, *J. Phys. Chem.* **1992**, *96*, 10591 – 10594; b) R. A. Reed, R. Purrello, K. Prendergast, T. G. Spiro, *J. Phys. Chem.* **1991**, *95*, 9720 – 9727; c) M. S. Liao, S. Scheiner, *J. Chem. Phys.* **2002**, *117*, 205 – 219.

[11] a) S. C. Jeoung, D. Kim, D. W. Cho, *J. Raman Spectrosc.* **2000**, *31*, 319 – 330; b) V. A. Walters, J. C. Depaula, G. T. Babcock, G. E. Leroi, *J. Am. Chem. Soc.* **1989**, *111*, 8300 – 8302.

